Improvement Performance of Standalone PV System Based on a New Quadratic Boost Converter

Zainab A. Ghafour*‡ (iD), Ahmed R. Ajel** (iD), Naseer M. Yasin*** (iD)

[1,2,3] Department of Electrical power Engineering Techniques, Middle Technical University, Electrical Engineering Technical College, Baghdad, Iraq

(eng.zainab777@gmail.com, dr_ahmed.R@mtu.edu.iq, naseeryasin@yahoo.com)

‡Corresponding Author 1. Zainab A. Ghafour, Baghdad, Iraq; Tel: +9647727441105,

eng.zainab777@gmail.com

Abstract- Numerous studies are being conducted to design more effective photovoltaic (PV) systems that use DC/DC converters. The design of a new quadratic boost for use in PV applications is discussed in this study. The design is based on an incremental conductance (INC) in the maximum power point tracking (MPPT) method. An improved architecture is used in this type of boost, and it can deliver a high conversion voltage ratio despite having low duty cycle values. The suggested topology is controlled by a hard switching signal derived from PWM and has a variable duty cycle based on the MPPT algorithm. The practical verification has been completed, and the INC algorithm has been programmed onto Arduino Nano. The quadratic boost converter (QBC) is verified in real-time using an actual PV module. The simulation and experiments' results validated the proposed topology's practicality for use in PV applications.

Keywords: quadratic boost, photovoltaic (PV), maximum power point tracking (MPPT), standalone system.

1. Introduction

Photovoltaic (PV) energy is a renewable energy source with much potential and has been garnering more and more attention recently. PV has several benefits, like being clean, quiet, and not requiring any maintenance. On the other hand, it has a few drawbacks associated with the PV cells' efficiency, the sun's variable nature, and its reliance on environmental factors, particularly solar temperature and irradiance. Voltage and current production from photovoltaic modules are frequently relatively high; nevertheless, they can only generate their maximum power when operated at a single combination of current and voltage values. It is common practice to place an algorithm-controlled DC-DC converter (MPPT) between the PV panels and the load, as depicted in figure 1 [1,2]. This is done to monitor the maximum power point (MPP) at any given time and ensure that the impedances of the PV module and the load are equal [3].

In recent decades, power electronics have experienced a development that has contributed to the enhancement of DC-DC converters, DC-AC inverters, and PV systems.

The primary objective of making use of DC-DC converters is to raise or lower the DC voltage that is being supplied by the photovoltaic arrays in order to achieve MPPT. The power switching devices in a typical PWM should ideally operate at maximal switching frequencies to ensure a more comprehensive conversion range. This is the case in most ordinary PWM converters. This operation seeks to offer the converter with the lowest or most excellent available duty ratios. However, the power switching devices' limited commutation times, switching surges, and operating frequencies limit their capacity to do so [4-6]. A solution suggested in [7,8] was to use n-stages coupled with a cascade and one active switch. As a result, there would be no need for complicated control circuitry, and the massive switching losses at each level would be reduced. The quadratic boost converter, sometimes known as the QBC, is the subject of this work. It combines two boosts that are chained together using a single active switch. For this particular topology, electromagnetic interference is reduced in QBC compared to cascaded linked boost, and the output ripple is improved in QBC based on power phase shifting [9-11].

This paper proposed a new quadratic boost converter with higher output, higher efficiency, and lower ripple than a conventional boost converter. The creation of a DC-DC converter with high efficiency and high gain ratio with low ripple in current and voltage will boost the dc voltage from solar energy under various weather situations, then converted by a single-phase inverter interfaced by a simple controller microcontroller to produce a pure sinusoidal AC voltage according to the grid voltage and frequency.

2. Proposed PV Configuration of a two-stage System

Figure 1 depicts a schematic representation of a system configuration that includes PV panels, a DC-DC converter connected by a single-phase inverter bridge, and an LC filter. The output voltage and the current via the inductor are regulated by a pair of regulators that have been implemented. The two-loop control scheme aims to have a low steady-state error while achieving a fast transient reaction and sufficient margin for stability.
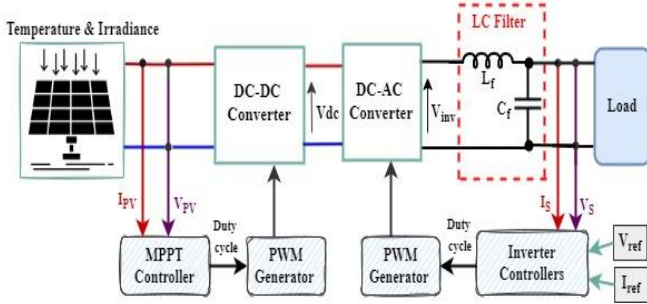

Fig.1. The proposed system.

3. Solar Photovoltaic Array

As depicted in Fig. 1, an ideal model of a PV solar cell consists of an ideal current source connected to an ideal diode. Many solar cells are connected in parallel and series to form a photovoltaic array. Series resistance (Rs) is more prevalent in PV modules, but shunt resistance (Rsh), which is extremely big, is considered infinite. The open-circuit voltage (Vo.c) increases as solar insolation increases, while the Vo.c falls when the temperature rises. As the temperature rises, the bandgap energy requires more energy to traverse the bandgap, lowering the PV cell's efficiency [12, 13].
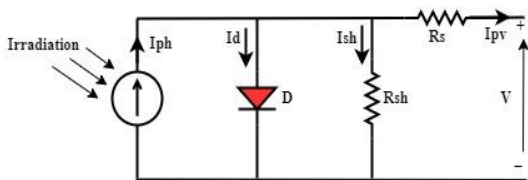

**Fig.2.** The electrical circuit of the equivalent PV cell.

The specification of the PV panel that use in the system is listed in Table (I)

**Table 1.** PV panel specifications used in the system

Parameter	Value
Maximum Peak Voltage (V_{mp})	18.55 V
Maximum Peak Current (I_{mp})	8.25 A
Open Circuit Voltage (V_{oc})	22.20 V
Short Circuit Voltage (I_{SC})	8.81 A
Maximum Power (P_m)	150 W
Number of cells	36

4. Converter The Proposed New Configuration Of The DC-DC

The proposed (QBC) consists of two inductors (L1, L2), three capacitors (C1, C2, Co), four diodes (D1, D2, D3, Do), , and one switch (S). The proposed converter has a simple structure with high gain ratio than the literature review mentioned in the introduction. The sections below discuss the analysis of the proposed converter. The configuration of the proposed circuit can be illustrated in Fig. 3(a).
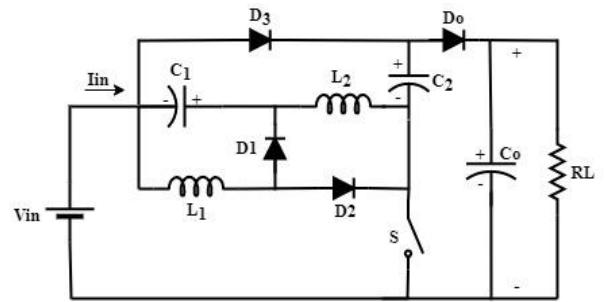
(a)
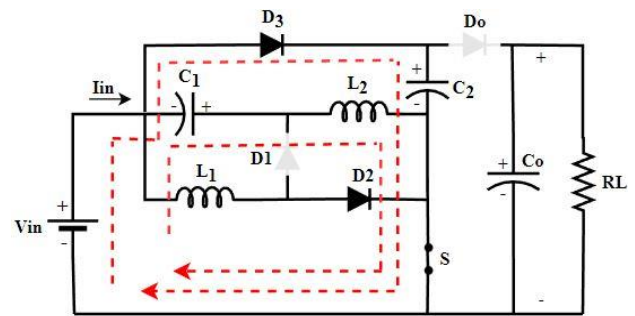
(b)
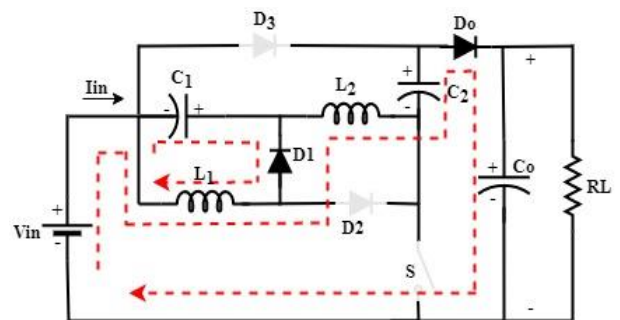
(c)

Fig.3. (a) The Equivalent Circuit of the proposed Converter (b) Switch (ON), (c) Switch (OFF).

The main objective of this converter is to increase the output voltage and efficiency and achieve high reliability. The operation of this converter is divided into three modes:

Mode I: When the switch (S) is turned ON, the inductors (L1) and capacitor (C2) are connected in parallel with the voltage source (Vin) through the diodes (D2, D3) for charging the capacitors and inductors as depicted in Fig. 3(b). At the

same time, the inductor (L1) is charged in series with the input source plus the voltage across the capacitor (C1). The diodes (D1) and the output diode (DO) are reverse biased. Also, in this period, the output capacitor (CO) discharges its stored energy to the load.

Mode II: When the switch (S) is turned OFF, the inductors (L2) and capacitors (C2) are connected in series, and the inductor (L1) is discharged in parallel with the voltage source (Vin) through the output diode (DO) to discharge the stored energy to charge the output capacitor (CO) and provide energy to the load. The diodes (D2, D3) are reverse biased, and the output diode (DO) and (D1) are forward-biased, as depicted in figure 3(c).

When the switch (S) is turned ON, the switching period time is ($t_{on} = D\,T$), the passive elements (L1, C1) are charged by Vin, and the inductors current during this period increases to reach maximum value. The voltage across the capacitor and inductor during this interval time can be expressed by applying the KVL law:

$$\left.\begin{array}{l} V_{L1} = V_{in} \\ V_{L2} = V_{in} + V_{C1} \\ V_{C2} = V_{in} \end{array}\right\} \tag{1}$$

when the switch (S) is turned off, the switching period duration is and the inductor's current falls throughout this time. The following is achieved by using (KVL):

$$V_{L1} = V_{C1} \tag{2}$$

$$V_{in} + V_{C1} + V_{L2} + V_{C2} - V_O = 0 \tag{3}$$

$$V_{L2} = V_O - 2\,V_{in} - V_{C1} \tag{4}$$

$$V_{L1}T_{ON} = V_{L1}T_{OFF} \tag{5}$$

Where, $T_{ON} = DT$ and $T_{OFF} = (1-D)T$

$$V_{C1} = \frac{D\,V_{in}}{1-D} \tag{6}$$

The following equations are produced using the voltage–second balance principle across the inductor equation

$$V_{L2}T_{ON} = V_{L2}T_{OFF} \tag{7}$$

$$(V_{in} + V_{C1})\,DT = (V_O - 2V_{in} - V_{C1})\,(1-D)\,T \tag{8}$$

As a result, equation (3.40) gives the following relationship for the voltage transfer ratio:

$$\frac{V_o}{V_{in}} = \frac{(1-D)^2+1}{(1-D)^2} \tag{9}$$

The suggested converter circuit's voltage transfer ratio gain (M_{ccm}) in CCM is:

$$M_{CCM} = \frac{V_o}{V_{in}} = \frac{(1-D)^2+1}{(1-D)^2} \tag{10}$$

Also, because all passive elements and semiconductor devices are perfect, the input power (Pin) and output power

(Pout) is equal, $p_o = p_{in}$, the output current (I_o) equals ($I_o = \frac{V_o}{R}$). As a result, the input current (I_{in}) can be calculated as:

$$I_{in} = \frac{(1-D)^2+1}{(1-D)^2}I_o = \frac{(1-D)^2+1}{(1-D)^2}\frac{V_o}{R} \tag{11}$$

The value of inductor L_1 & L2 are calculated using the formula,

$$L_1 = \frac{V_{in}D}{F_s\,\Delta iL_1} \tag{12}$$

$$L_2 = \frac{V_{in}\,D}{F_s\,\Delta iL_2(1-D)} \tag{13}$$

The value of capacitors C1, C2, and Co are calculated using the formula,

$$C_O = \frac{V_O D}{R\,F_s\,\Delta V_O} \tag{14}$$

$$C_1 = \frac{V_O(1-2D)}{RF_s\,\Delta V_{C1}(1-D)} \tag{15}$$

$$C_2 = \frac{I_{in}(1-D)^2}{((1-D)^2+1)F_s\,\Delta V_{C2}} \tag{16}$$

Equations give the voltage stress across diodes and the MOSFET (S)

$$V_{do} = -(V_O - V_{in}) \tag{17}$$

During the OFF switch, the voltage stress across D_3 is:

$$V_{d3} = -(V_O - V_{in}) = V_{do} \tag{18}$$

The voltage stress across the D1 during the ON switch is:

$$V_{d1} = \frac{-V_{in}}{1-D} \tag{19}$$

During the OFF switch, the voltage stress across the MOSFET and D_2 are:

$$V_S = V_O - V_{in} \tag{20}$$

$$V_{d2} = \frac{D}{(1-D)^2}V_{in} \tag{21}$$

5. Incremental Conductance (INC) Algorithm

Since the efficiency of solar cells is affected by changing weather conditions, an MPPT controller that works with a DC-DC converter was used to obtain the maximum power from the solar cells. In this paper, the incremental conductance algorithm was used. The input to the INC algorithm is the current and the voltage of the photocell. This algorithm differs in its design from P&O. The INC method is less oscillatory than P&O because higher oscillations affect the output power of the P&O method. This approach requires the controller to perform more calculations, but it can track changing conditions faster than the P&O technique. This technique uses the photovoltaic array's incremental conductivity (I/ΔV) to calculate the relationship between variation in power with voltage (ΔP/V).

The INC algorithm compares the incremental conductance (ΔI/ΔV) with the array conductance (I/V) to get the maximum power point. When these two are equal, the output voltage is

the MPP voltage ($\Delta I/\Delta V=I/V$). The controller keeps this voltage constant until the irradiation changes, and the procedure is repeated.

The primary objective of this algorithm is to find the operating voltage point where the conductivity equals the additional discharge. The use of the INC algorithm enhances the functionality of the system (current, voltage, power). The proposed approach improves the system's stability and accuracy while shortening response times, and a few oscillations to eventually arrive at a greater value when the variation of the duty cycle (D) with the proposed, system has better stability. And, therefore the INC method has a short response time and minimizes oscillation around the MPP compared with the P&O algorithm. Fig. 4 shows a flowchart of the incremental algorithm [14, 15]
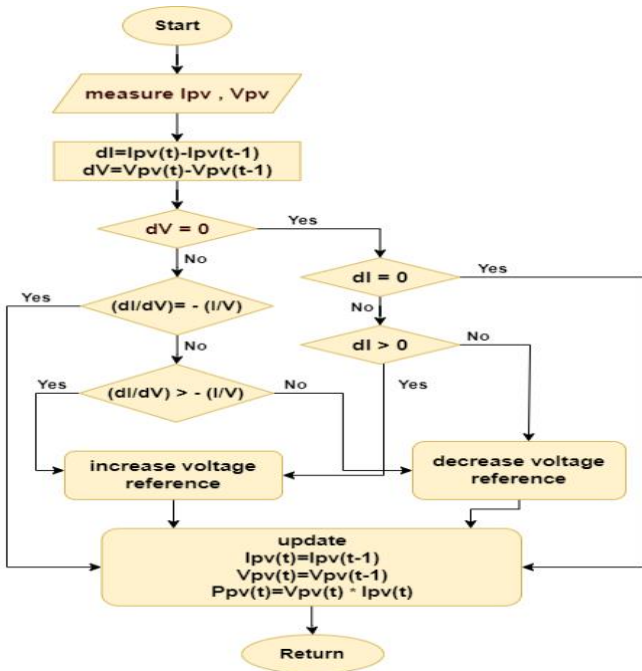

Fig .4. The INC algorithm flowchart.

6. AC Side Inverter Control

Figure 5 shows the model diagram of the inverter and the two-loop control system. In order to improve the resonance damping and ensure the safety of the power circuit, a proportional controller called Gi(s) was implemented in the internal current loop, and the voltage controller Gv(s), tracks the voltage reference with a quick response during transitions and a small amount of inaccuracy during steady state operation. To improve the shape of the waves in terms of current, voltage, and energy, the currents are controlled to control the stability of the voltage. The Gi(s) and Gv(s) are PI controllers.
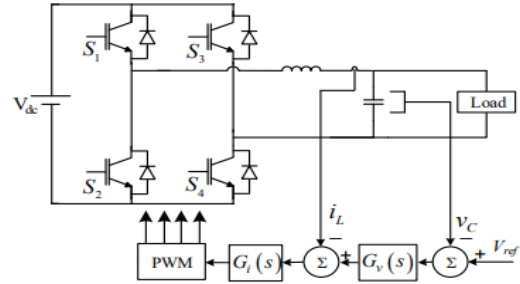

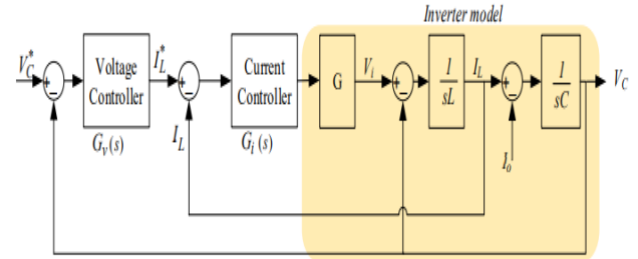**Fig. 5**. Inverter with a control structure.

Fig. 6. Scheme of two loop control with inverter model.

The inner loop is required based on the PI controller to keep the output voltage of the inverter at the load side constant. The error of comparison between the reference and actual voltage is the PI controller to minimize it to zero. The output of the PI controller is a reference current, as demonstrated in Fig. 6. The actual current is compared with the reference current, and the output error enters the voltage controller, a PI controller, to produce a sinusoidal waveform. This wave is compared with a saw tooth carrier waveform to produce suitable gate pulses to the four switches of the inverter. The Gv(s) voltage controller is designed to supply all the different loads with a constant sinusoidal voltage [16-18].

7. Simulation and Experimental Results

In order to determine whether or not the proposed topology was suitable for the system, a hardware prototype of the component of the system topology was created and put through its paces in the lab, as shown in Fig. 7(a,b, and c). The Arduino Nano was chosen to serve as the control unit. It is responsible for producing four SPWM signals and then transmitting them to the TLP350 driver. The Arduino Nano and the driver require some power for the external power supply to accomplish their jobs. Thus the necessary 5V and 15V DC power were supplied. Four pulse width modulation signals were sent to the IGBTs via the Driver Unit. The off-grid single-phase inverter was used in this work.

In addition, the suggested converter test parameters have been developed following the equations mentioned above. As a result, the values of the components utilized in the design are presented in Table (II). The proposed converter is designed for photovoltaic solar-powered dc applications. The duty ratio is kept at 0.5, and the converter's input voltage is 18.5 V in order to evaluate the converter's performance through simulation and experiment., and the output is (92) V in the proposed

converter, The converter voltage is 92 volts, but a test was made by increasing the duty cycle until the converter voltage was increased to 150 volts, as shown in the simulation and experimental results in figures 8 and 9. This is done so that the performance of the converter can be evaluated. A load, a voltage source, an Arduino controller, and a converter are the components that make up each device. MOSFETs are typically used for switching circuits. The frequency of the converter will be set to 50 kilohertz at this time. The newly presented converters all functioned at CCM, and the basic experimental waveforms of the measured voltage and the power MOSFET were presented in Fig. 10.

The voltage waves that can be seen across the diodes and inductors are depicted in Figs. 11, 12, and 13, respectively. In addition, we note the agreement between the theoretical predictions and the experimental findings, which compare the input and output voltages in actual use, waves of duty cycle, and the voltage across inductors and each diode.

The functionality of the SPWM inverter hardware prototype is used to gather data to perform performance analysis. The information was gathered for the load of the AC lighting. Arduino Nano produced two SPWM signals (VG1 and VG3), which were then sent to the four gate drivers (TLP 350). The gate drivers were responsible for automatically generating the alternate SPWM signals (VG2 and VG4). After then, these four SPWM signals were sent to the four IGBTs so that they could be used for switching. The simulation and experimental findings for the proposed Standalone inverter are shown in Figs. 14, 15, 16, 17, and 18. These figures detailed the inverter voltage, current, and power consumption of the hardware prototype and simulation of the system when it was linked with AC loads. This proposed topology yields a pure sinusoidal result at 50 Hz. In Figs. 15, 16, 17 and 18, the waves are shown before using the filter and after using the filter, as it was used to filter the waves from the harmonics (voltage and current) coming out of the inverter. The output power of the inverter according to the output waves in Figs. 15, 16 is 600W, the rated RMS voltage is about 100V and the rated RMS current is 6A. the proposed converter is very suitable for the standalone transformerless system. The experimental results in the figures are similar to the simulated results, but there is a difference in the gradations of the waveforms as shown in Fig. 18 of the paper, and this result is compatible with the simulation results. The simulation and experiment results demonstrate that the suggested converter works well with the transformerless standalone system.

Table 2. The proposed system's parameters

Parameter	Value
Quadratic boost capacitor (C_1)	100 µf
Output capacitor (C_2)	100 µf
Duty cycle (D)	0.5
Input current ripple (ΔI)	$0.3 \times Vin$
Output voltage ripple (ΔV)	$0.005 \times Vo$
Operation frequency (f)	50 Hz
Switching frequency (fs)	50Khz
Efficiency	97.4%
Rated power of inverter (Pacinv)	600W
Minimum input voltage (Vin $_{min}$)	18.5V
DC-DC converters output (V_{out})	110V
P_{Load}	145W
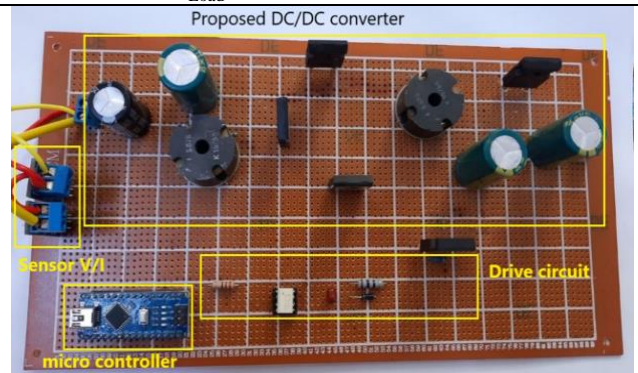
(a)
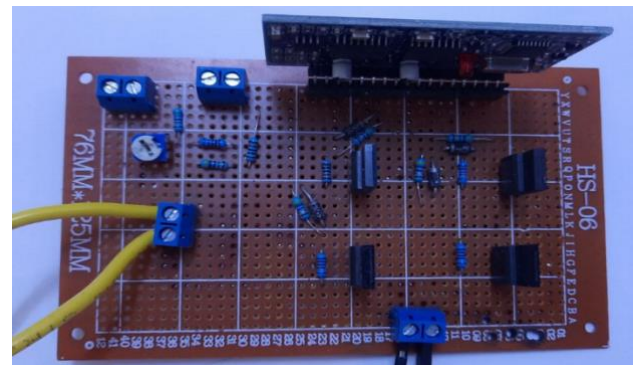
(b)
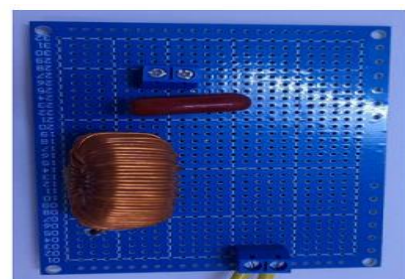
(c)

Fig. 7. Prototype of (a) new quadratic boost converter, (b) AC side, and (c) LC filter.
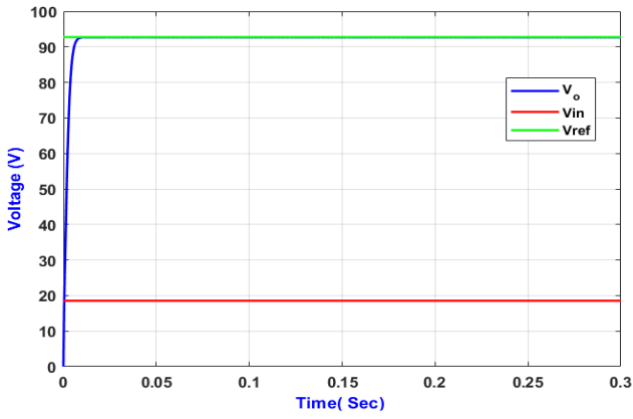
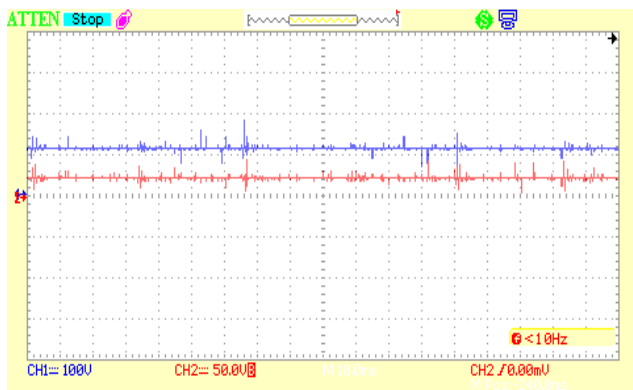**Fig. 8.** Simulation response of input and output voltage of QBC.

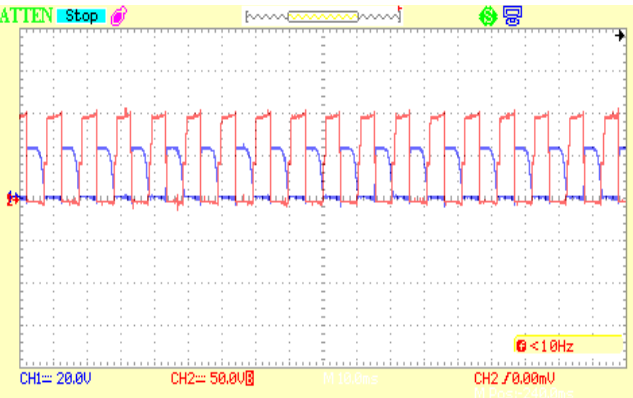**Fig.9.** Response of output and input voltages of the proposed converter.

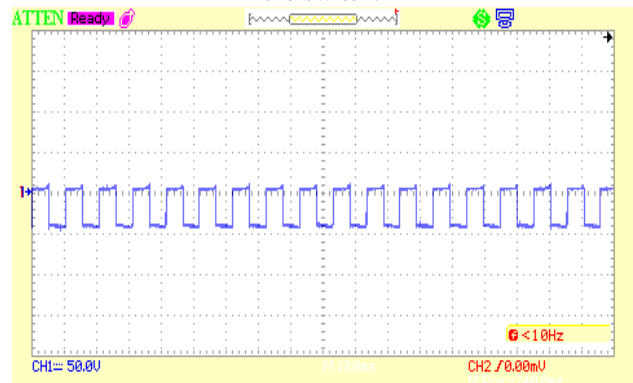**Fig. 10.** Gate pulses of MOSFET and voltage stress across the switch.

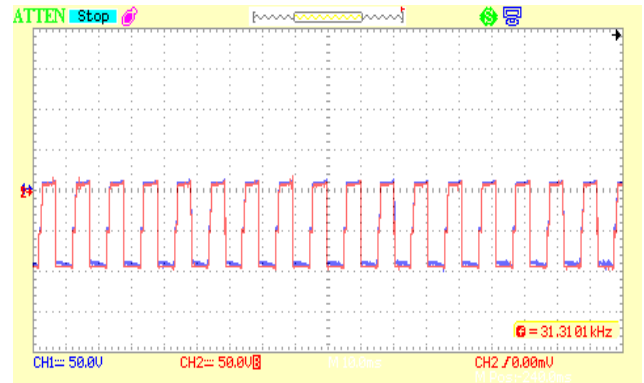**Fig. 11.** Voltage stress across the diode (V_{D1}).

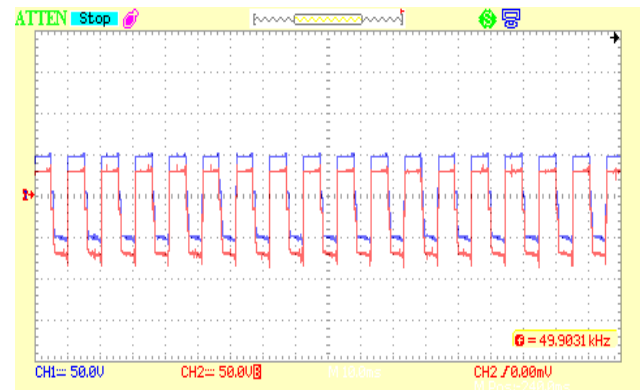**Fig. 12.** Voltage stress across the diode (V_{D3} & V_{D0}).

Fig. 13. Voltage stress across the diode (V_{L1} & V_{L2}).
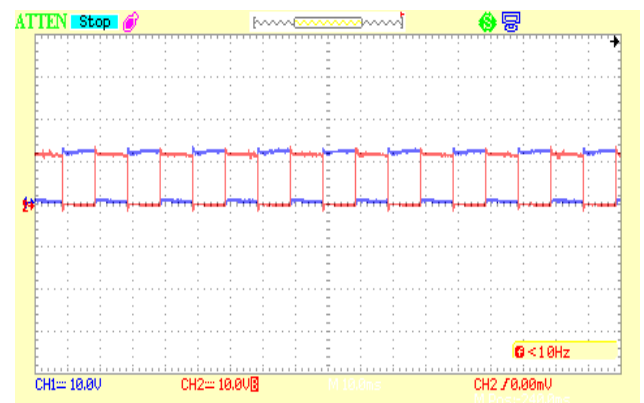

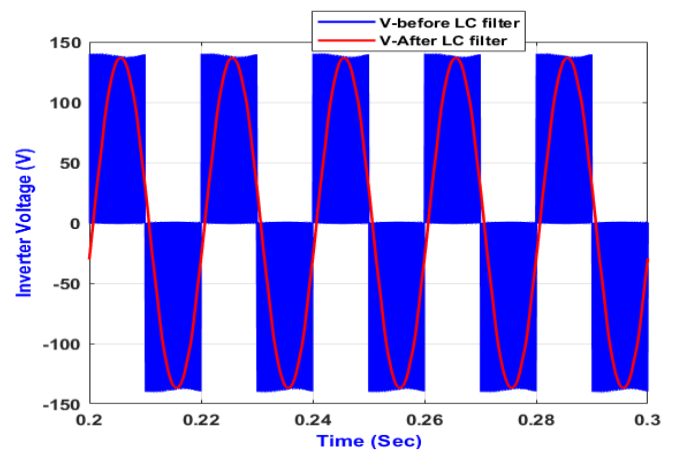**Fig. 14.** Gate pulses of the inverter.

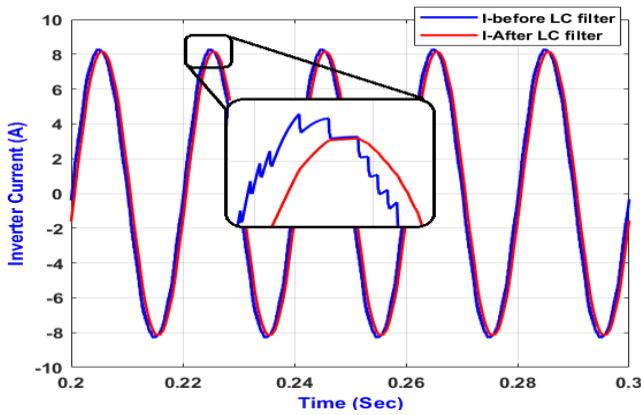**Fig. 15.** Simulation outcome of the inverter voltage.

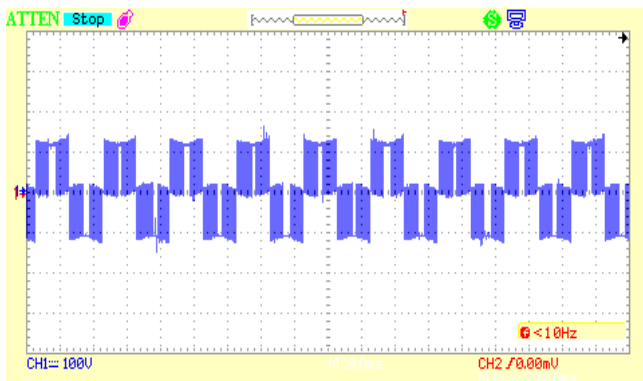**Fig. 16.** Inverter current with and without LC filter.

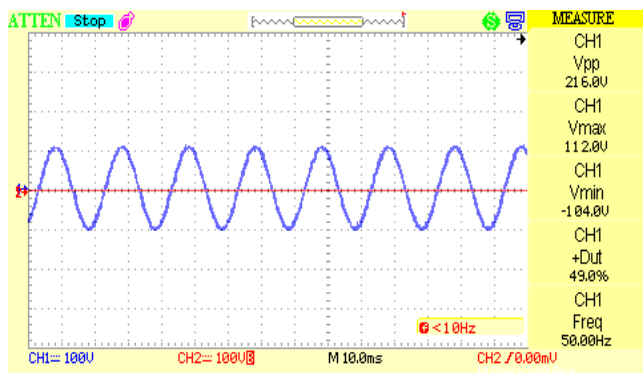**Fig. 17.** Inverter terminals output voltage without the filter.

Fig. 18. AC voltage across the load with the filter.

8. Conclusion

The quadratic boost topology of the DC/DC converter was experimentally tested for an actual MPPT PV system in this particular piece of research. It combines the proposed converter with a single-phase inverter under AC load. The performance of the INC MPPT algorithm was examined while the ambient circumstances were held constant. The experimental system was put through its paces with rapid changes in the amount of solar irradiation. Constant monitoring and real-time provision of the highest PV power available ensured that the electrical load was met. The experimental verification was carried out without any problems. The findings appear pleasing, demonstrating that the quadratic boost converter is ultimately convenient for PV applications. The hardware results are matching with the theoretical results. One can use other control techniques to improve the performance of the proposed application. Therefore, this study can be extended to utilize these recent control schemes [19-24].

References

[1]   Y. Amara, R. Boukenoui, R. Bradai, and H. Salhi, "Design and control of two-stage standalone photovoltaic generation system," in *2018 International Conference on Communications and Electrical Engineering (ICCEE)*, 2018: IEEE, pp. 1-5.

[2]   M. Y. Ali Khan, H. Liu, Z. Yang, and X. Yuan, "A comprehensive review on grid connected photovoltaic inverters, their modulation techniques, and control strategies," *Energies,* vol. 13, no. 16, p. 4185, 2020.

[3]   M. J. Hasan and F. A. M. Al-Qrimli, "Single-Phase, H-Bridge 3-level Inverter of Wide Range Input Voltage for Grid Connected Solar Photovoltaic Applications," *International Journal of Computer Applications,* vol. 975, p. 8887.

[4]   M. Darameičikas *et al.*, "Design of a DC-DC converter in residential solar photovoltaic system," in *Journal of Physics: Conference Series*, 2019, vol. 1174, no. 1: IOP Publishing, p. 012006.

[5]   P. Selvabharathi, S. Veerakumar, and V. K. Kannan, "Simulation Of Dc-Dc Converter Topology For Solar Pv System Under Varying Climatic Conditions With Mppt Controller," in *IOP Conference Series: Materials Science and Engineering*, 2021, vol. 1084, no. 1: IOP Publishing, p. 012084.

[6]   S. Saravanan and N. Ramesh Babu, "A modified high step-up non-isolated DC-DC converter for PV application," *Journal of applied research and technology,* vol. 15, no. 3, pp. 242-249, 2017.

[7]   Y. Liu, J. Wang, and H. Tu, "Design and implementation of finite time nonsingular fast terminal sliding mode control for a novel high step-up DC-DC converter," *Energies,* vol. 12, no. 9, p. 1716, 2019.

[8]   J. Ai and M. Lin, "High step-up DC–DC converter with low power device voltage stress for a distributed generation system," *IET Power Electronics,* vol. 11, no. 12, pp. 1955-1963, 2018.

[9]   A. Nakpin and S. Khwan-on, "A novel high step-up DC-DC converter for photovoltaic applications," *Procedia Computer Science,* vol. 86, pp. 409-412, 2016.

[10]   J. D. Navamani, A. Geetha, D. Almakhles, A. Lavanya, and J. S. M. Ali, "Modified LUO High Gain DC-DC Converter With Minimal Capacitor

Stress for Electric Vehicle Application," *IEEE Access,* vol. 9, pp. 122335-122350, 2021.

[11] D. Murali, "Steady State Behavior of a Single-Switch Non-isolated DC-DC SEPIC Converter Topology with Improved Static Voltage Gain," *Journal Européen des Systèmes Automatisés,* vol. 54, no. 3, pp. 445-452, 2021.

[12] J. M. Home-Ortiz, O. D. Melgar-Dominguez, J. R. S. Mantovani, and J. P. Catalão, "PV hosting capacity assessment in distribution systems considering resilience enhancement," *Sustainable Energy, Grids and Networks,* vol. 32, p. 100829, 2022.

[13] A. O. Baba, G. Liu, and X. Chen, "Classification and evaluation review of maximum power point tracking methods," *Sustainable Futures,* vol. 2, p. 100020, 2020.

[14] M. H. Uddin, M. A. Baig, and M. Ali, "Comparision of 'perturb & observe'and' incremental conductance', maximum power point tracking algorithms on real environmental conditions," in *2016 International Conference on Computing, Electronic and Electrical Engineering (ICE Cube)*, 2016: IEEE, pp. 313-317.

[15] H. Chen, Y. Cui, Y. Zhao, and Z. Wang, "Comparison of P&O and INC Methods in Maximum Power Point Tracker for PV Systems," in *IOP Conference Series: Materials Science and Engineering*, 2018, vol. 322, no. 7: IOP Publishing, p. 072029.

[16] S. Bera, S. Chakraborty, D. Kumar, N. Ali, and M. Lehtonen, "Optimal deep learning based aggregation of TCLs in an inverter fed standalone microgrid for voltage unbalance mitigation," *Electric Power Systems Research,* vol. 210, p. 108178, 2022.

[17] B. E. Elnaghi, M. E. Dessouki, M. Abd-Alwahab, and E. E. Elkholy, "Development and implementation of two-stage boost converter for single-phase inverter without transformer for PV systems," *International Journal of Electrical & Computer Engineering (2088-8708),* vol. 10, no. 1, 2020.

[18] S. Semeskandeh, M. Hojjat, and M. Hosseini Abardeh, "Techno–economic–environmental feasibility study of a photovoltaic system in northern part of Iran including a two-stage multi-string inverter with DC–DC ZETA converter and a modified P&O algorithm," *Clean Energy,* vol. 6, no. 1, pp. 891-904, 2022.

[19] N. SUSHMI and D. Subbulekshmi, "Robust Solar Irradiation Forecasting Mechanism for Maximum Power Point Trackers: A Comparative Review," *International Journal of Renewable Energy Research (IJRER),* vol. 12, no. 4, pp. 1846-1870, 2022.

[20] P. A. Nagoro, T. Tarmizi, and I. D. Sara, "Cascaded Multilevel Inverter with Minimum Number of Conducting Switches and Using Capacitor Compensation," *International Journal of Renewable Energy Research (IJRER),* vol. 12, no. 4, pp. 1980-1987, 2022.

[21] H. V. P. Nguyen and T. T. Huynh, "Comparative Efficiency Assessment Of MPPT Algorithms In Photovoltaic Systems," *International Journal of Renewable Energy Research (IJRER),* vol. 12, no. 4, pp. 2061-2067, 2022.

[22] R. R. Udumula, P. S. R. Kotana, H. B. SK, and S. Goud, "High Gain Boost Converter Fed Single-Phase Sine Pulse Width Modulated Inverter," *International Journal of Renewable Energy Research (IJRER),* vol. 12, no. 2, pp. 659-666, 2022.

[23] S. BENHADOUGA, A. BELKAID, R. FARHAN, M. MEDDAD, and A. Eddiaif, "Experimental Comparative Study MPPT between P&O and Sliding Control of a Small PV System," *International Journal of Renewable Energy Research (IJRER),* vol. 12, no. 2, pp. 863-869, 2022.

[24] Z. A. Ghafour, A. R. Ajel, and N. M. Yasin, "A New High Gain Quadratic DC-DC Boost Converter for Photovoltaic Applications," in *2022 10th International Conference on Smart Grid (icSmartGrid)*, 2022: IEEE, pp. 137-144.